Active nematics with quenched disorder

Sameer Kumar* and Shradha Mishra†
Indian Institute of Technology (BHU), Varanasi, Uttar Pradesh 221005, India

(Received 3 March 2020; revised 27 July 2020; accepted 2 November 2020; published 25 November 2020)

We introduce a two-dimensional active nematic with quenched disorder. We write the coarse-grained hydrodynamic equations of motion for slow variables, viz. density and orientation. Disorder strength is tuned from zero to large values. Results from the numerical solution of equations of motion as well as the calculation of two-point orientation correlation function using linear approximation shows that the ordered steady state follows a disorder dependent crossover from quasi-long-range order to short-range order. Such crossover is due to the pinning of $\pm 1/2$ topological defects in the presence of finite disorder, which breaks the system in uncorrelated domains. Finite disorder slows the dynamics of $+1/2$ defect, and it leads to slower growth dynamics. The two-point correlation functions for the density and orientation fields show good dynamic scaling but no static scaling for the different disorder strengths. Our findings can motivate experimentalists to verify the results and find applications in living and artificial apolar systems in the presence of a quenched disorder.

DOI: 10.1103/PhysRevE.102.052609

I. INTRODUCTION

Dynamics and steady state of a collection of active self-propelled particles with different kinds of inhomogeneities has become an interesting area of research [1–7]. Recent studies have mostly focused on the polar self-propelled particles in the presence of inhomogeneous agents or medium [8–10]. The effect of disorder in active polar particles introduces many exciting features, which, in general, do not present in the corresponding equilibrium system of the same symmetry [11]. Studies on the effect of disorder in apolar particles are limited to the equilibrium system only [12]. Disorders are present almost everywhere in active apolar systems [1], but ordering and steady state of active apolar particles with the disorder is rarely studied.

Variety of systems where particles have head-tail symmetry, like vibrated granular rods [13,14], collection of molecular motors, cytoskeletal filaments [15,16], mesenchymal, epithelial cells monolayers [17–20], bacterial colonies [21–23], and colonies of swarming filamentous bacteria [24] are a few examples of the active apolar system. The collection of such active apolar particles, forming an orientationally ordered state, is called active nematics. Most of the previous active nematic studies are for a clean system [25–28]. But, inhomogeneity or disorder can play a crucial role in steady state and kinetics of active nematics, which is our current study's focus.

In this paper, we study quenched disorder's effect on a collection of active apolar particles on a two-dimensional substrate. The disorder introduced as a random field of strength h_0 in the coarse-grained hydrodynamic equations of motion for slow variables are local density $\rho(\mathbf{r}, t)$ and order parameter $\mathcal{Q}(\mathbf{r}, t)$. We first characterize the steady state and then study the ordering kinetics. We calculate the nematic order parameter (NOP) $\mathbf{Q}$ vs system size N for different h_0. For clean or homogeneous active nematic, NOP decay algebraically with N [quasi-long-range order (QLRO)]. But, for a finite disorder, NOP shows a power-law decay, for small N, and a disorder dependent crossover to an exponential decay [short-range order (SRO)] for large N, and the same we confirm by the calculation of two-point orientation correlation function in the steady state, using a linear approximation. The origin of such crossover for the finite disorder ($h_0 \neq 0$) is due to the pinning of the $\pm 1/2$ defects. For large enough N, it breaks the system in uncorrelated domains, and the size of these domains depends on the disorder strength. Although the orientation field is significantly affected due to disorder, the density fluctuation remains unaffected and shows the usual giant number fluctuation (GNF) [26,27,29] for all disorder strengths (h_0).

We also studied the effect of disorder on the dynamics of the defects and the ordering kinetics. The *effective* dynamic growth exponent, z_{eff} [30], increases on increasing disorder. The two-point correlation functions for both fields show good dynamics scaling for all disorder, but no static scaling is found for different disorder.

We organize the paper as follows. We introduce the model of our system in Sec. II. In Sec. III, we discuss the steady-state properties, then we discuss defect dynamics and system kinetics in Sec. IV; further, in Sec. V, we calculate the two-point correlation functions. We summarize the results in Sec. VI.

II. MODEL AND NUMERICAL DETAILS

We construct a monolayer of self-propelled apolar particles of length l, on a two-dimensional substrate of friction coefficient χ. Each particle is driven by an inherent driving force

*sameerk.rs.phy16@itbhu.ac.in
†smishra.phy@itbhu.ac.in

F acting along the particle's long axis. The ratio of the force F to the friction coefficient gives a constant self-propulsion speed $v_0 = F/\chi$ to each particle. The apolar nature of the particle makes them move forward and backward with *equal* probability with a step size equal to v_0. On a time scale, large compared to the interaction time, and length scale much larger than the particle size, the dynamics of the system is governed by coupled hydrodynamic equations of motion for slow variables, viz. local density $\rho(\mathbf{r}, t)$, and local NOP $\mathcal{Q}(\mathbf{r}, t)$ [31],

$$\partial_t \rho = a_0 \nabla_i \nabla_j \rho \mathcal{Q}_{ij} + D\rho \nabla^2 \rho, \tag{1}$$

$$\partial_t \mathcal{Q}_{ij} = [\alpha_1(\rho) - \alpha_2(\mathcal{Q} : \mathcal{Q})]\mathcal{Q}_{ij} + \beta\left(\nabla_i \nabla_j - \tfrac{1}{2}\delta_{ij}\nabla^2\right)\rho + D_{\mathcal{Q}}\nabla^2 \mathcal{Q}_{ij} + H_{ij} + \Omega_{ij}. \tag{2}$$

Equations (1) and (2) are written in dimensionless units by rescaling all lengths by the length of the particle and time by the collision time and are of the same form as derived from the microscopic rule-based model in [25], with an additional term due to *quenched disorder*. The quenched disorder is introduced as a *random field* in the free energy density $\mathcal{F} = -\mathcal{Q} : (\mathbf{hh} - \frac{\mathbf{I}}{2})$, which further leads to $H_{ij} = (h_i h_j - h_0^2 \frac{1}{2}\delta_{ij})$; in Eq. (2), in two dimensions $i, j = 1, 2$ are the spatial indices for the two components of vectors, where $h_i = h_0(\cos\phi, \sin\phi)$—here h_0 is the disorder strength and $\phi(\mathbf{r})$ is a uniform random angle between $(0, 2\pi)$, with mean zero, quenched in time (no time dependence) and space correlation $\langle \phi(\mathbf{r})\phi(\mathbf{r}')\rangle = \delta(\mathbf{r} - \mathbf{r}')$.

The last term Ω_{ij} is a tensorial symmetric traceless white noise with mean zero, such that $\langle \Omega_{ij}(\mathbf{r}, t)\Omega_{kl}(\mathbf{r}', t')\rangle = \Delta_0 \delta(\mathbf{r} - \mathbf{r}')\delta(t - t')\epsilon_{ijkl}$. Here, Δ_0 is the noise strength and $\epsilon_{ijkl} = \frac{1}{2}(\delta_{ik}\delta_{jl} + \delta_{il}\delta_{jk} - \delta_{ij}\delta_{kl})$.

In the above Eqs. (1) and (2) we keep the model minimal and ignore the flow field [32], completely, or assume the interaction among the particle is short range volume exclusion, and no hydrodynamic interaction. Hence the system we study is *dry* active nematic.

The random field introduced in our current model is similar to the random field in XY model (RFXY model) [11]. Hereafter we refer to our model as random field active nematic (RFAN) when $h_0 \neq 0$ and clean-active nematic (clean-AN) for $h_0 = 0$.

To perform the numerical integration of Eqs. (1) and (2) we construct a two-dimensional $K \times K$ square lattice with periodic boundary condition (PBC) and discretize the space and time derivatives using Euler scheme ($\Delta x = 1.0$ and $\Delta t = 0.1$). Initially, we start with random homogeneous density, with mean ($\rho_0 = 0.75$), and random orientation.

We first study the steady state of the system for $h_0 = (0.0, 0.15)$ and system size, i.e., $K = 64$–512. Coarsening is studied for larger $K = 1024$. Steady-state results are obtained for simulation time $t = O(10^6)$ and the average over 10 independent realisations. One simulation time is counted after update of Eqs. (1) and (2) for all lattice points. Parameters in Eqs. (1) and (2) are ($a_0 = 0.1$–0.3), $D_\rho = \frac{1}{4}(a_0^2 + 1)$, $\rho_0 = 0.75$, $\rho_c = 0.5$, $\alpha_2 = 1$, $\beta = 0.25$, and $D_{\mathcal{Q}} = 1$, $\Delta_0 = 10^{-4}$ and we check that the system remains stable for the chosen set of parameters.

III. STEADY-STATE PROPERTIES

We first measure the steady-state properties of RFAN for different h_0. The global ordering in the system is measured by calculating the nematic order parameter (NOP) defined as $\mathbf{Q} = \langle \frac{1}{N}\sqrt{|\sum_{i=1}^{N}\cos(2\theta_i)|^2 + |\sum_{i=1}^{N}\sin(2\theta_i)|^2}\rangle$, where the sum runs over all the lattice points. $\langle \ldots \rangle$ shows the average over many realizations. We compare the measured $\mathbf{Q}$ in numerical simulation with the analytical expression for the two-point orientation correlation function $C_{\mathcal{Q}}$ [Eq. (3)], obtained from a linearized treatment of small fluctuation in a uniform ordered phase. We calculate the equal time Fourier transformed spatial correlation of angle $S_{\mathbf{q}}(\theta)$ as a function of wave vector $\mathbf{q}$ and present our result for $q_x = q_y$. Starting from the equations of motion (1) and (2), a straightforward linearized approximation shows that, for a finite disorder strength,

$$C_{\mathcal{Q}}(N) \simeq \frac{1}{N^{\mathcal{B}'}} e^{-\mathcal{C}' h_0^4 N}, \tag{3}$$

which is obtained from the inverse Fourier transform of orientation structure factor $S_{\mathbf{q}}(\theta)$ at wave number $q \simeq N^{-1/2}$. The coefficients in Eq. (3), $\mathcal{B}' = 1.17 \times 10^{-4}$ and $\mathcal{C}' = 3.9 \times 10^{-3}$ (for $a_0 = 0.2$), are constants and depend on the system parameters. Hence $C_{\mathbf{Q}}$ is a product of algebraic and exponential decay with N. Figure 1(a) data points show the plot of NOP vs N for different disorder strengths, h_0. For clean AN, $\mathbf{Q}$ decays algebraically as N^{-B}, where $B \simeq 1.05 \times 10^{-4}$ depends on system parameters. Also, B is small, since, for the given parameters, clean AN is in the deep ordered state and significantly away from the isotropic-nematic transition, where it shows the instability [33–36]. For finite disorder, $\mathbf{Q}$ shows the deviation from the pure algebraic decay. It decays algebraically for small N and leads a crossover to exponential decay for a larger N. The larger the disorder strength, the crossover to exponential decay appears for smaller N.

In Fig. 1(a) lines are a plot of $\sqrt{C_{\mathcal{Q}}(N, h_0)}$, Eq. (3). For clean AN, $C_{\mathcal{Q}}(N, 0)$ is pure power law, whereas, for RFAN, it decays exponentially for higher N. Hence crossover happens after a disorder dependent N, $N_c(h_0) \sim h_0^{-4}$. We find a good match of lines [Eq. (3)] and data from the simulation. We see a systematic deviation between data points from the simulation and the linear study lines for large h_0, which is due to nonlinearities present in the model. In Fig. 1(b) we plot the $\mathbf{Q} \times N^{\mathcal{B}'/2}$ vs $N \times h_0^4$ for different h_0 and find a good collapse of data for different disorder strengths.

To further understand the steady state in RFAN, we calculate the probability distribution function (PDF) $P(\Delta\theta)$ of angle fluctuations $\Delta\theta$ from the mean direction. Figure 1(c) shows the plot of $P(\Delta\theta)$ vs $\Delta\theta$ for different (h_0, a_0). $P(\Delta\theta)$ for clean AN shows a very narrow peak at $\Delta\theta = 0$, whereas, for RFAN, PDF has a much broader distribution and more than one peak at nonzero $\Delta\theta$ (see the Appendix for snapshots). Lines in Fig. 1(c) are fit to two distinct peaks for $h_0 = 0.05$, $a_0 = 0.3$ with Gaussian. On increasing activity, the width of the distribution sharpens, and more distinct peaks emerge. Hence it infers the stronger intradomain ordering and distinct ordered domains for large activity. Similarly, for a more considerable disorder, $P(\Delta\theta)$ shows a greater number of such different peaks, which means that smaller domains

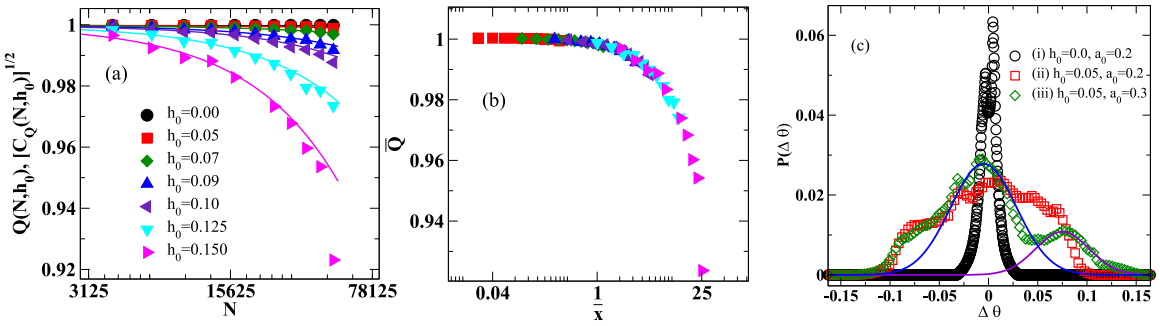

FIG. 1. (a) NOP $\mathbf{Q}$ vs system size $N = K \times K$ for different h_0 (symbols) and $\sqrt{C_Q}$, Eq. (3) (solid lines). (b) Scaled NOP, $\bar{Q} = Q \times N^{\mathcal{B}'/2}$ vs $\bar{x} = N \times {h_0}^4$. (c) Probability distribution function $P(\Delta\theta)$ of angle fluctuations of angular orientation for different values of (h_0, a_0), i.e., $(0.0, 0.2)$, $(0.05, 0.2)$, and $(0.05, 0.3)$. Data for $h_0 = 0.05$, $a_0 = 0.3$ (data points) fitted with Gaussian for two distinct peaks (solid lines).

emerge more if we further increase the disorder strength (data not shown).

In the Appendix and the Supplemental Material (SM) (see the Supplemental Materiel [37]), we show the animation for the snapshots of local NOP for clean $h_0 = 0.05$ and $h_0 = 0.1$, which shows that, for a clean system, the final state is globally ordered, whereas, for RFAN, different ordered domains are formed and survived at late times.

We also calculate the steady-state density fluctuation, for all disorder, number fluctuation $\sigma = \sqrt{\langle {N_s}^2 \rangle - \langle N_s \rangle^2} \sim \langle N_s \rangle$, where N_s is the mean number of particle in subcells, Fig. 2, which shows a giant number fluctuation (GNF), as found in [26,27,29]. When compared with the linearized calculation of two-point density structure factor, as given in Eq. (36), for $q \simeq N^{-1/2}$, density fluctuation should show the fluctuations larger than the clean AN. But large fluctuation can arise for size $N_s > N_c \sim h_0^{-4}$, which is hard to achieve in numerical simulation. Hence, in general, inhomogeneity does not affect the density fluctuations in active nematic, although it significantly changes the nature of two-point orientation correlation function. Now we further study the ordering kinetics to such a steady state.

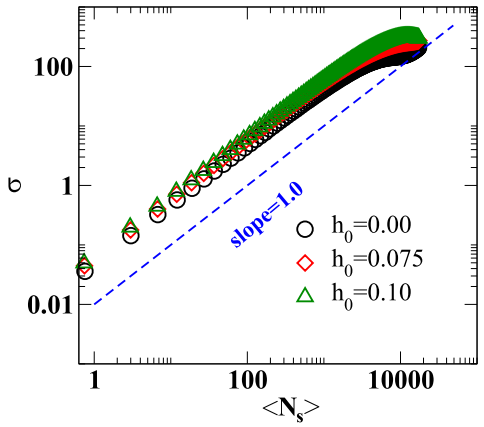

FIG. 2. Number fluctuation σ vs $\langle N_s \rangle$ plot for different disorder strengths and $K = 300$.

IV. KINETICS

A. Defect dynamics

When the system is brought from a disordered state to an ordered state, ordering happens through the process of domain formation and which is due to the creation and annihilation of $\pm 1/2$ topological defects.

In the two-dimensional active nematic, these defects have topological geometry [38]. A $+1/2$ defect has a cometlike structure and moves along the axis parallel to its tail, whereas a $-1/2$ defect has a threefold symmetry and does not have any preferred direction of motion [32,39,40]. The dynamics of defects play a vital role in the ordering of the system [30]. In Figs. 3(a) and 3(b), we study the dynamics of defects for a clean AN ($h_0 = 0.0$), as well as for RFAN ($h_0 = 0.075$). Figure 3(a) shows the snapshots of local NOP, $\mathcal{Q}$, for clean AN (upper panel) and RFAN (lower panel). White arrows show the relative separation, $\Delta r(t)$, between a pair of $\pm 1/2$ defects. The arrow's tail and head represent the position of $+1/2$ and $-1/2$ defects, respectively. We see that the disorder slows the dynamics of the $+1/2$. The variation of $\Delta r(t)$ vs time is shown in Fig. 3(b). The length of the white arrow in Fig. 3(a) decreases with time [or Δr decays with time, Fig. 3(b)], which shows the two defects coming close to each other. For clean AN, $\Delta r(t)$ decay at a faster rate, whereas it takes a longer time in the presence of disorder. Hence the relative speed is small in the presence of disorder, as shown in the inset of Fig. 3(b). To further understand the mechanism of slowing down of defect dynamics, in Figs. 3(c) and 3(d), we show the snapshot of the local density current near a pair of $\pm 1/2$ defects. Density current $\mathbf{J}_\rho$ is defined from Eq. (1), which can be rewritten as a continuity equation, $\partial_t \rho = -\nabla \cdot \mathbf{J}_\rho$, where $\mathbf{J}_\rho = -a_0 \nabla \cdot (\rho \mathcal{Q}) - D_\rho \nabla \rho$. The intensity of colors shows the magnitude of the density current. For clean AN, current flow is smooth near the defects, Fig. 3(c), whereas with disorder ($h_0 = 0.075$), current flow is distorted, Fig. 3(d), which results in slower growth dynamics, which we will discuss next. We also studied the effect of activity on the relative speed of a pair of defects. For larger activity, the relative separation (starting from the same relative separation) between a pair of defects decreases faster, and hence they annihilate quickly, which, in turn, results in more ordering for the same disorder strength (see the Appendix for details).

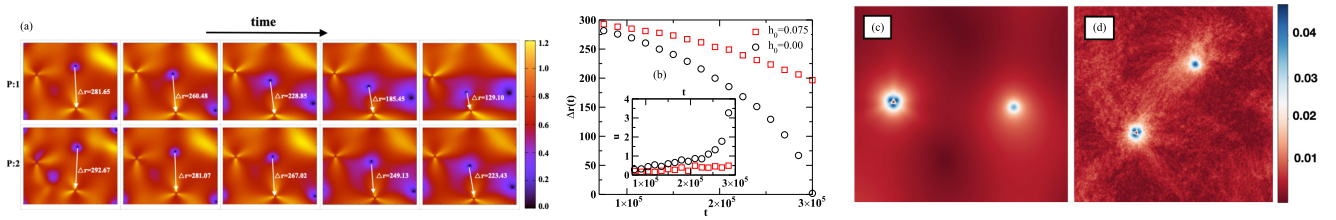

FIG. 3. (a) Snapshots of local NOP $\mathcal{Q}$: upper panel (P:1) is for clean AN (i.e., $h_0 = 0.0$) and bottom panel (P:2) is for RFAN ($h_0 = 0.075$) and the number along the white arrow is the relative separation [$\Delta r(t)$] between the + and $-1/2$ defects. (b) $\Delta r(t)$ vs t plot for $h_0 = 0.0, 0.075$. u is the relative speed of defects defined as $u = |\frac{d}{dt}\Delta r(t)| \times 10^{-3}$ and plotted in the inset of (b). (c) Snapshot of density current near the defects for clean AN, $h_0 = 0.0$ and (d) RFAN, $h_0 = 0.075$. Intensity of colors shows the magnitude of the density current. Data is generated for system size $N = 512^2$.

B. Growth law and scaling properties

As we discussed in the previous paragraph, disorder affects the defect dynamics, and it can further influence the kinetics of domain ordering. We characterize the domain growth by calculating the correlation functions for orientation $\mathcal{Q}$, $C_{\mathcal{Q}}(\mathbf{r}, t) = \langle \mathcal{Q}(\mathbf{0}, t) : \mathcal{Q}(\mathbf{r}, t)\rangle$, and local density ρ, $C_\rho(\mathbf{r}, t) = \langle \delta\rho(\mathbf{0}, t)\delta\rho(\mathbf{r}, t)\rangle$, where $\delta\rho(\mathbf{r}, t) = \rho(\mathbf{r}, t) - \rho_0$ is the deviation of the local density from the mean ρ_0. With time both correlations increase due to domain growth. Figures 4(a) and 4(b) show the plot of $C_{\mathcal{Q}}(r/L(t))$ and $C_\rho(r/L(t))$ vs scaled distance $r/L_{\mathcal{Q},\rho}(t)$ and they all collapse to a single curve, where the characteristic length $L_{\mathcal{Q},\rho}(t)$ is calculated from the first zero crossing of $C_{\mathcal{Q}}(\mathbf{r}, t)$ and $C_\rho(\mathbf{r}, t)$. Figures 4(c) and 4(d) show the plot of $C_{\mathcal{Q}}(r/L_{\mathcal{Q}}(t))$ and $C_\rho(r/L_\rho(t))$ vs scaled distance $r/L_{\mathcal{Q},\rho}(t)$ calculated at equal time ($t = 10^5$) for different disorder h_0. We find no scaling for different disorder strengths for both $\mathcal{Q}$ and ρ. Therefore, for all disorder strengths, the system shows good dynamic scaling but no static scaling in orientation and density.

The equilibrium analog of clean AN is XY model and the characteristic length of growing domain in two-dimensional XY model goes as $L_{XY}(t) \sim [t/\ln(t)]^{1/2}$ [30,41]. Hence we assume that, for RFAN, $L_{\mathcal{Q},\rho} \sim [t/\ln(t)]^{1/z_{\text{eff},\mathcal{Q},\rho}}$ and further calculate the dynamics growth exponent $z_{\text{eff},\mathcal{Q},\rho}$ from correlation length $L_{\mathcal{Q},\rho}(t)$, defined as $\frac{1}{z_{\text{eff},\mathcal{Q},\rho}} = \langle \frac{d \ln L_{\mathcal{Q},\rho}(t)}{d(t/\ln t)} \rangle$ [30,40–42], where $\langle \ldots \rangle$ is the mean value of z_{eff} over intermediate time ($t \sim 1000$ to 15 000) when it remains constant for at least one decade; see Fig. 5(a). We find that $z_{\text{eff},\mathcal{Q},\rho} \simeq 2$ for clean AN and increases on increasing h_0. In Fig. 5(b), we plot the $\Delta z = z_{\text{eff}} - 2$ vs h_0 on log - log scale. The change Δz increases algebraically with h_0 with power $\sim$2 and $\sim$1 for $\mathcal{Q}$ and ρ, respectively. Hence growth kinetics of density field show small change in comparison to orientation field. Or small change in growth kinetics of density field affects the orientation field substantially.

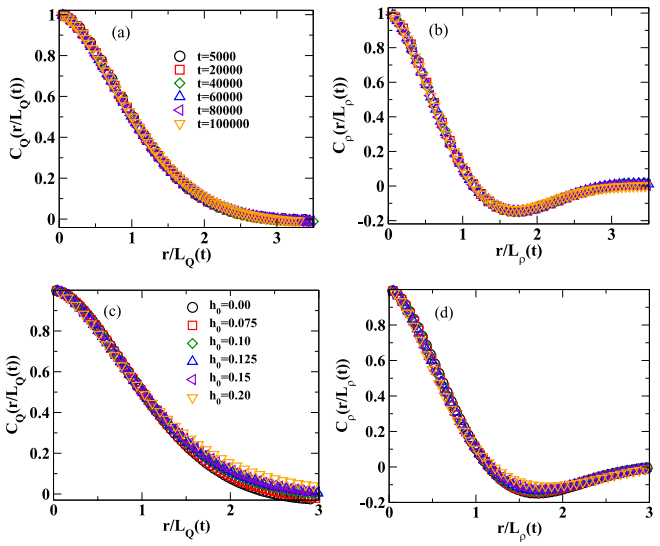

FIG. 4. Two-point correlation function $C_{\mathcal{Q},\rho}$ vs scaled distance $r/L_{\mathcal{Q},\rho}(t)$. (a),(b) Two-point correlation function for RFAN, i.e., $h_0 = 0.1$, at different simulation time (t). (c),(d) Two-point correlation function for different h_0 and at fixed simulation time $t = 10^5$.

C. Morphology of ordered domains

We study the effect of disorder on the morphology of ordering domains. We calculate the behavior of scaled two-point correlation functions $C_{\mathcal{Q},\rho}(r/L_{\mathcal{Q},\rho})$ for small $r/L_{\mathcal{Q},\rho}$. In the limit of small $r/L_{\mathcal{Q},\rho}$, $C_{\mathcal{Q},\rho}(r/L_{\mathcal{Q},\rho}) \sim 1 - (\frac{r}{L_{\mathcal{Q},\rho}})^\alpha$, where α is called the cusp exponent and features the domain morphology [30,43]. In Fig. 6 we plot the $1 - C_{\mathcal{Q},\rho}(r/L_{\mathcal{Q},\rho})$ vs scaled distance $r/L_{\mathcal{Q},\rho}$ on log - log scale and estimate the cusp exponent α for both fields ($\mathcal{Q}$, ρ). The exponent $\alpha \simeq 1.7$ for both fields and for all disorder strengths. Hence domain morphology remains unaffected in the presence of disorder.

V. LINEARIZED HYDRODYNAMIC CALCULATION OF TWO-POINT CORRELATION FUNCTIONS

We start with the hydrodynamic equations of motion for local density ρ and NOP $\mathcal{Q}$ as introduced in Eqs. (1) and (2),

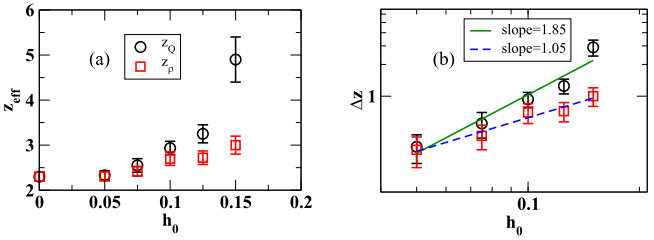

FIG. 5. Plots of dynamic growth exponent $z_{\text{eff}}(h_0)$ vs disorder strength h_0 (a) and Δz vs h_0 on log - log scale (b).

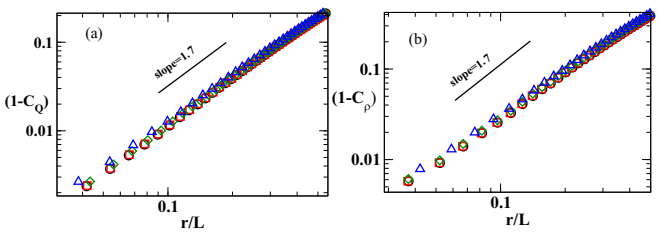

FIG. 6. Cusp's exponent α (slope of the plot) for Q and ρ field. Diffrent symbols used for different values of disorder strength: $h_0 = 0.0$ (circle), $h_0 = 0.05$ (square), $h_0 = 0.075$ (diamond), and $h_0 = 0.10$ (triangle).

First, two terms on the right-hand side (RHS) of Eq. (2) are the mean-field terms: $\alpha_1(\rho) = \alpha_0(\frac{\rho}{\rho_c} - 1)$, where ρ_c is the critical density and where $\alpha_0 = 1$ is chosen as unity for simplicity. The system shows a homogeneous ordered state for $\alpha_1(\rho_0) > 0$ and disordered isotropic state when $\alpha_1(\rho_0) < 0$, where ρ_0 is the mean density of particles. The third term is coupling to the density field and the fourth term is the diffusion in $\mathcal{Q}$. Origin of such diffusion can be obtained from the equal elastic constant approximation of Frank-free energy for a two-dimensional equilibrium nematic [44,45].

We rewrite Eqs. (1) and (2) neglecting the higher order fluctuations about the homogeneous ordered steady state. The local nematic order parameter $\mathcal{Q}$ is given as $\mathcal{Q} = \frac{S}{2}\begin{bmatrix}\cos 2\theta & \sin 2\theta \\ \sin 2\theta & -\cos 2\theta\end{bmatrix}$, where S is a scalar and a measure of ordering. We define $\delta\rho$, δS, and θ as the fluctuation terms from their mean values ρ_0, S_0, and θ_0, respectively. Here, $S_0 = \sqrt{\frac{2\alpha_1(\rho_0)}{\alpha_2}}$, and is obtained from Eq. (2), main text, for the homogeneous steady state. Therefore, to linear order we have $\mathcal{Q}_{11} = \frac{1}{2}(S_0 + \delta S)$, $\mathcal{Q}_{12} = \theta S_0$, and Eq. (1), main text, gives

$$\partial_t(\rho_0 + \delta\rho) = a_0\left[\partial_x{}^2(\rho_0 + \delta\rho)\frac{(S_0 + \delta S)}{2} + \partial_y{}^2(\rho_0 + \delta\rho)\frac{[-(S_0 + \delta S)]}{2} + 2\partial_x\partial_y(\rho_0 + \delta\rho)S_0\theta\right] + D_\rho\nabla^2(\rho_0 + \delta\rho) \tag{4}$$

or

$$\partial_t\delta\rho = a_0\left[\partial_x^2\frac{(S_0\delta\rho + \rho_0\delta S)}{2} - \partial_y^2\frac{(S_0\delta\rho + \rho_0\delta S)}{2} + 2S_0\rho_0\partial_x\partial_y\theta\right] + D_\rho\left(\partial_x^2 + \partial_y^2\right)\delta\rho \tag{5}$$

or

$$\partial_t\delta\rho = \left(\frac{a_0S_0}{2} + D_\rho\right)\partial_x^2\delta\rho + \left(D_\rho - \frac{a_0S_0}{2}\right)\partial_y^2\delta\rho + \frac{a_0\rho_0}{2}\left(\partial_x^2 - \partial_y^2\right)\delta S + 2a_0\rho_0S_0\partial_x\partial_y\theta, \tag{6}$$

while the equation for δS [Eq. (2), main text] in homogeneous steady state gives

$$0 = \left[\alpha_1(\rho_0) + \alpha_1{}'(\rho_0)\delta\rho - \frac{\alpha_2}{2}({S_0}^2 + 2S_0\delta S)\right]\frac{S_0 + \delta S}{2} + \cdots. \tag{7}$$

Also $\alpha_1(\rho_0) - \frac{\alpha_2}{2}{S_0}^2 = 0$. Therefore, we have

$$[\alpha_1{}'(\rho_0)\delta\rho - \alpha_2S_0\delta S](S_0 + \delta S) = 0, \tag{8}$$

$$\delta S = \frac{\alpha_1{}'(\rho_0)\delta\rho}{\alpha_2S_0}, \tag{9}$$

or

$$\delta S = \Gamma\delta\rho, \tag{10}$$

where $\Gamma = \frac{\alpha_1{}'(\rho_0)}{\alpha_2S_0}$ and $\alpha_1{}' = \frac{\partial\alpha_1(\rho)}{\partial\rho}|_{\rho=\rho_0}$. Hence Eq. (6) can be rewritten as

$$\partial_t\delta\rho = \left(\frac{a_0S_0}{2} + D_\rho\right)\partial_x^2\delta\rho + \left(D_\rho - \frac{a_0S_0}{2}\right)\partial_y^2\delta\rho + \frac{a_0\rho_0}{2}\Gamma\left(\partial_x^2 - \partial_y^2\right)\delta\rho + 2a_0\rho_0S_0\partial_x\partial_y\theta \tag{11}$$

or

$$\partial_t\delta\rho = \left(\frac{a_0S_0}{2} + D_\rho + \Gamma\frac{a_0\rho_0}{2}\right)\partial_x^2\delta\rho + \left(-\frac{a_0S_0}{2} + D_\rho - \Gamma\frac{a_0\rho_0}{2}\right)\partial_y^2\delta\rho + 2a_0\rho_0S_0\partial_x\partial_y\theta \tag{12}$$

or

$$\partial_t\delta\rho = K_1\partial_x^2\delta\rho + K_2\partial_y^2\delta\rho + K_3\partial_x\partial_y\theta, \tag{13}$$

where $K_1 = (\frac{a_0S_0}{2} + D_\rho + \Gamma\frac{a_0\rho_0}{2})$, $K_2 = (-\frac{a_0S_0}{2} + D_\rho - \Gamma\frac{a_0\rho_0}{2})$, and $K_3 = 2a_0\rho_0S_0$.

Now the equation of motion for $\mathcal{Q}_{12}$,

$$\partial_t \mathcal{Q}_{12} = [\alpha_1(\rho) - \alpha_2(\mathcal{Q}:\mathcal{Q})]\mathcal{Q}_{12} + \beta\left(\nabla_1\nabla_2 - \tfrac{1}{2}\delta_{12}\nabla^2\right)\rho + D_{\mathcal{Q}}\nabla^2\mathcal{Q}_{12} + H_{12} + \Omega_{12}. \tag{14}$$

Here, $\mathcal{Q}_{12} = S_0\theta$; therefore, in linear order, $[\alpha_1(\rho) - \alpha_2(\mathcal{Q}:\mathcal{Q})]\mathcal{Q}_{12}$ will not survive. $h_1h_2 = {h_0}^2\cos\phi\sin\phi = {h_0}^2\Phi(\mathbf{r})$, where $\Phi(\mathbf{r}) = \cos\phi\sin\phi$:

$$\partial_t\theta = \frac{\beta}{\rho_0 S_0}\partial_x\partial_y\delta\rho + D_{\mathcal{Q}}\left(\partial_x^2 + \partial_y^2\right)\theta + \frac{{h_0}^2}{\rho_0 S_0}\Phi + \frac{1}{\rho_0 S_0}\Omega. \tag{15}$$

Taking the Fourier transform of Eqs. (13) and (15), where Fourier modes are defined as $f(\mathbf{q},\omega) = \iint f(\mathbf{r},t)e^{i\mathbf{q}\cdot\mathbf{r}+i\omega t}d\mathbf{r}\,dt$, we get

$$(K_1{q_x}^2 + K_2{q_y}^2 - i\omega)\delta\rho(\mathbf{q},\omega) + K_3 q_x q_y\theta(\mathbf{q},\omega) = 0 \tag{16}$$

and

$$\frac{\beta}{\rho_0 S_0}q_x q_y\delta\rho(\mathbf{q},\omega) + [D_{\mathcal{Q}}({q_x}^2 + {q_y}^2) - i\omega]\theta(\mathbf{q},\omega) = \frac{{h_0}^2}{\rho S_0}\Phi(\mathbf{q}) + \frac{1}{\rho S_0}\tilde{\Omega}(\mathbf{q},\omega). \tag{17}$$

Solving Eqs. (16) and (17) will give

$$\mathbf{M}\begin{bmatrix}\delta\rho(\mathbf{q},\omega)\\ \theta(\mathbf{q},\omega)\end{bmatrix} = \frac{1}{\rho_0 S_0}\begin{bmatrix}0\\ {h_0}^2\Phi(\mathbf{q}) + \tilde{\Omega}(\mathbf{q},\omega)\end{bmatrix}, \tag{18}$$

where

$$\mathbf{M} = \begin{bmatrix}K_1{q_x}^2 + K_2{q_y}^2 - i\omega & K_3 q_x q_y\\ \frac{\beta}{\rho_0 S_0}q_x q_y & D_{\mathcal{Q}}({q_x}^2 + {q_y}^2) - i\omega\end{bmatrix}. \tag{19}$$

By solving Eq. (18) for $q_x = q_y$, we get

$$\begin{bmatrix}\delta\rho(\mathbf{q},\omega)\\ \theta(\mathbf{q},\omega)\end{bmatrix} = \frac{1}{(D_1q^4 + \omega^2) - i\omega D_2q^2}\begin{bmatrix}-K_3q^2\\ 2D_\rho q^2 - i\omega\end{bmatrix}\frac{[{h_0}^2\Phi(\mathbf{q}) + \tilde{\Omega}(\mathbf{q},\omega)]}{\rho_0 S_0}, \tag{20}$$

where $D_1 = 4D_\rho D_{\mathcal{Q}} + 2a_0\beta$ and $D_2 = 2(D_\rho + D_{\mathcal{Q}})$. Equation (20) gives

$$\delta\rho(\mathbf{q},\omega) = \frac{-K_3q^2}{(D_1q^4 + \omega^2) - i\omega D_2q^2}\frac{[h_0^2\Phi(\mathbf{q}) + \tilde{\Omega}(\mathbf{q},\omega)]}{\rho_0 S_0}, \tag{21}$$

$$\theta(\mathbf{q},\omega) = \frac{2D_\rho q^2 - i\omega}{(D_1q^4 + \omega^2) - i\omega D_2q^2}\frac{\left[h_0^2\Phi(\mathbf{q}) + \tilde{\Omega}(\mathbf{q},\omega)\right]}{\rho_0 S_0}. \tag{22}$$

Now, we first calculate the two point orientation correlation functions,

$$\langle\theta(\mathbf{q},\omega)\theta(-\mathbf{q},-\omega)\rangle = \frac{{D_\rho}^2q^4 + \omega^2}{(D_1q^4 + \omega^2)^2 + \omega^2{D_2}^2q^4}\frac{[h_0^4\langle\Phi(\mathbf{q})\Phi(-\mathbf{q})\rangle + \langle\tilde{\Omega}(\mathbf{q},\omega)\tilde{\Omega}(-\mathbf{q},-\omega)\rangle]}{\rho_0 S_0}. \tag{23}$$

Here $\langle\Phi(\mathbf{q})\Phi(-\mathbf{q})\rangle = \delta(\mathbf{q}+\mathbf{q})$ and $\langle\tilde{\Omega}(\mathbf{q},\omega)\tilde{\Omega}(-\mathbf{q},-\omega)\rangle = \Delta_0\delta(\mathbf{q}+\mathbf{q})\delta(\omega+\omega)$. Using this, we get

$$S_q(\theta) = \mathcal{C}(D_\rho, D_{\mathcal{Q}})\frac{h_0^4}{q^4} + \mathcal{B}(D_\rho, D_{\mathcal{Q}})\frac{1}{q^2}, \tag{24}$$

where $\mathcal{C}(D_\rho, D_{\mathcal{Q}}) = \frac{4{D_\rho}^2}{\rho_0 S_0(4D_\rho D_{\mathcal{Q}} + 2a_0\beta)^2}$ and $\mathcal{B}(D_\rho, D_{\mathcal{Q}}) = \frac{\pi\Delta_0}{2\rho_0 S_0}\frac{1}{c\sqrt{2(4b^2+c^2)}}[\frac{[2{D_\rho}^2 + c(\sqrt{4b^2+c^2}) - 2b^2]}{\sqrt{c(c-\sqrt{4b^2+c^2})+2b^2}} + \frac{[-2{D_\rho}^2 + c(\sqrt{4b^2+c^2}) + 2b^2]}{\sqrt{c(c+\sqrt{4b^2+c^2})+2b^2}}]$, where $b = \sqrt{2(2D_\rho D_{\mathcal{Q}} + a_0\beta)}$ and $c = \sqrt{2(D_\rho + D_{\mathcal{Q}})}$.

Hence the two point angle correlation function can be written as

$$S_q(\theta) \simeq \frac{\mathcal{B}}{q^2} + \frac{\mathcal{C}h_0^4}{q^4}. \tag{25}$$

Here, the coefficients $\mathcal{C}$ and $\mathcal{B}$ depend on system parameters. To get the two point correlation function for nematic order parameter $C_{\mathcal{Q}}(x) \simeq \exp[-G_\theta(x)]$ [44], where $G_\theta(x)$ is the inverse Fourier transform of $S_q(\theta)$, Eq. (25). Also, $G(x) = \mathcal{B}f(x) + \mathcal{C}h_0^4g(x)$, where

$$f(x) = \int_{2\pi/L}^{2\pi/a}\frac{d^2q}{4\pi^2}\frac{1 - e^{i\mathbf{q}\cdot\mathbf{x}}}{q^2} \simeq \ln(\Lambda|x|) \tag{26}$$

and

$$g(x) = \int_{2\pi/a}^{2\pi/L}\frac{dq}{q^3}\left[\frac{1}{2}\int_0^{2\pi}d\theta(1 - e^{iq|x|\cos\theta})\right] \tag{27}$$

or

$$g(x) = \int_{2\pi/a}^{2\pi/L} \frac{dq}{q}[1 - J_0(q|x|)]. \tag{28}$$

Here J_n is the nth order Bessel function [46]:

$$g(x) = |x|^2 \int_0^1 \frac{du[1 - J_0(u)]}{u^3} + |x|^2 \int_1^{\Lambda|x|} \frac{du}{u^3} - |x|^2 \int_1^{\Lambda|x|} \frac{du[J_0(u)]}{u^3}, \tag{29}$$

$$g(x) = |x|^2 A + |x|^2 \left[-\frac{1}{2}\left(1 - \frac{1}{\Lambda^2|x|^2}\right)\right] - |x|^2 \int_1^{2\pi/a|x|} \frac{du[J_0(u)]}{u^3}, \tag{30}$$

$$g(x) = |x|^2 \left(A - \frac{1}{2} - |x|^2 \int_1^{2\pi/a|x|} \frac{du[J_0(u)]}{u^3}\right), \tag{31}$$

$$g(x) = \frac{a^2}{2\pi^2} + |x|^2 \left(A - \frac{1}{2} - A'\right). \tag{32}$$

Here $A = \int_{2\pi/L}^{2\pi/a} \frac{1-J_0(u)}{u^3} du \simeq 1.2$ and $A' = \int_1^{2\pi/a|x|} \frac{J_0(u)}{u^3} du \simeq \int_0^{\infty} \frac{J_0(u)}{u^3} du \simeq 0.27$. Here, $a = 1$ is the lattice spacing:

$$g(x) = |x|^2 \times O(0.01). \tag{33}$$

Hence the orientation correlation function is given by

$$C(x) \simeq \frac{1}{|x|^{\mathcal{B}}} e^{-|x|^2 \times O(0.01) \times \mathcal{C} h_0^4}. \tag{34}$$

When measured on the scale of system size $N = K^2$, we get

$$C_{\mathcal{Q}}(N) \simeq \frac{1}{N^{\mathcal{B}'}} e^{-\mathcal{C}' h_0^4 N}. \tag{35}$$

Here, $\mathcal{B}' = 1.17 \times 10^{-4}$ and $\mathcal{C}' = 3.9 \times 10^{-3}$.

Similarly, structure factor for density can be calculated using Eq. (21) and given by

$$S_\rho(\mathbf{q}) = \gamma_1 \frac{h_0^4}{q^4} + \gamma_2 \frac{\Delta_0}{q^2}, \tag{36}$$

where $\gamma_1 = 0.5$ and $\gamma_2 = 0.4$ are constants and depend only on system parameters.

VI. SUMMARY

We studied two-dimensional dry active nematics with the quenched random disorder using the the hydrodynamic equations of motion for the slow fields, viz. density ρ and orientation $\mathcal{Q}$, in a coarse-grained description.

The study from the numerical solution of equations of motion and the linearized hydrodynamic calculation shows that the orientation correlation follows a crossover from QLRO (algebraic decay of correlation) to SRO (exponential decay). Such crossover occurs due to the pinning of $\pm 1/2$ defects in the presence of finite disorder, which breaks the system in domains of different orientations. The size of such domains decreases on increasing disorder. For clean as well as RFAN, number fluctuation is giant.

We also studied the approach to the steady state by (i) characterizing the dynamics of $\pm 1/2$ defects and (ii) calculation of the characteristic length of growing domains $L_{\mathcal{Q},\rho}(t)$. The slow dynamics of $+1/2$ defect leads to the slower domain growth in the presence of disorder. Although domain growth is slower in the presence of disorder, the two-point correlation function for both fields $C_{\rho,\mathcal{Q}}$ shows good dynamic scaling. Still, no static scaling is found for different disorder strengths. Domain morphology remains unaffected in the presence of disorder.

We find an interesting steady state in RFAN, which is different from its corresponding equilibrium counterpart: random field XY model [11]. Our study should motivate experimentalists to verify our findings and encourage us to study the effect of other kinds of disorders in active nematics. To make the model minimal, the effect of background fluid is ignored in our present study; hence it is for dry active nematic. It would be interesting to extend this study for wet active systems [32,47,48].

ACKNOWLEDGMENTS

S.M. would like to thank S. Ramaswamy and S. Puri for useful discussion at the beginning of the project. S.K. would like to thank M. Kumar, D. Giri, and R. Singh for useful suggestions. S.K. thanks IIT(BHU) Varanasi and SNBNCBS Kolkata for computational facility. S.M. and S.K. thank DST-SERB India, Grant No. ECR/2017/000659, for financial support.

APPENDIX: SNAPSHOTS FOR $\Delta\theta$ AND NOP

1. Snapshots for $\Delta\theta$

The snapshots corresponding to Fig. 1(c) are shown in Fig. 7. Here we can see that for a nonzero disorder in the

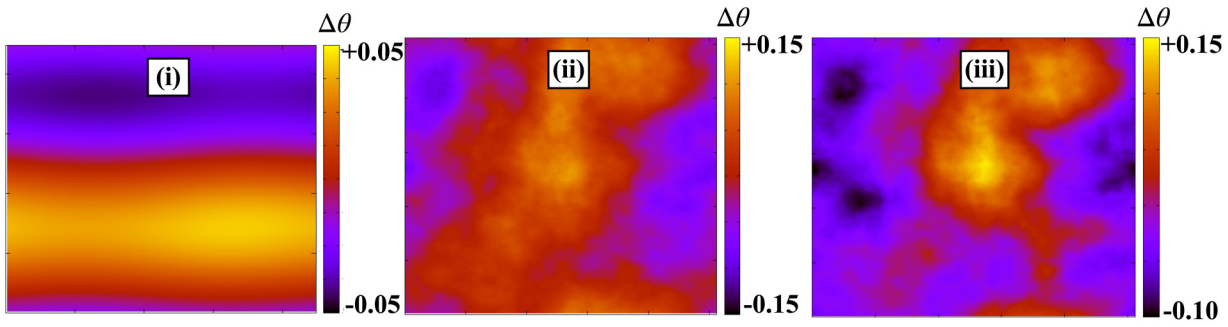

FIG. 7. Snapshots of $\Delta\theta$ for $h_0 = 0.0$, $a_0 = 0.2$ (i), $h_0 = 0.05$, $a_0 = 0.2$ (ii), and $h_0 = 0.05$, $a_0 = 0.3$ (iii).

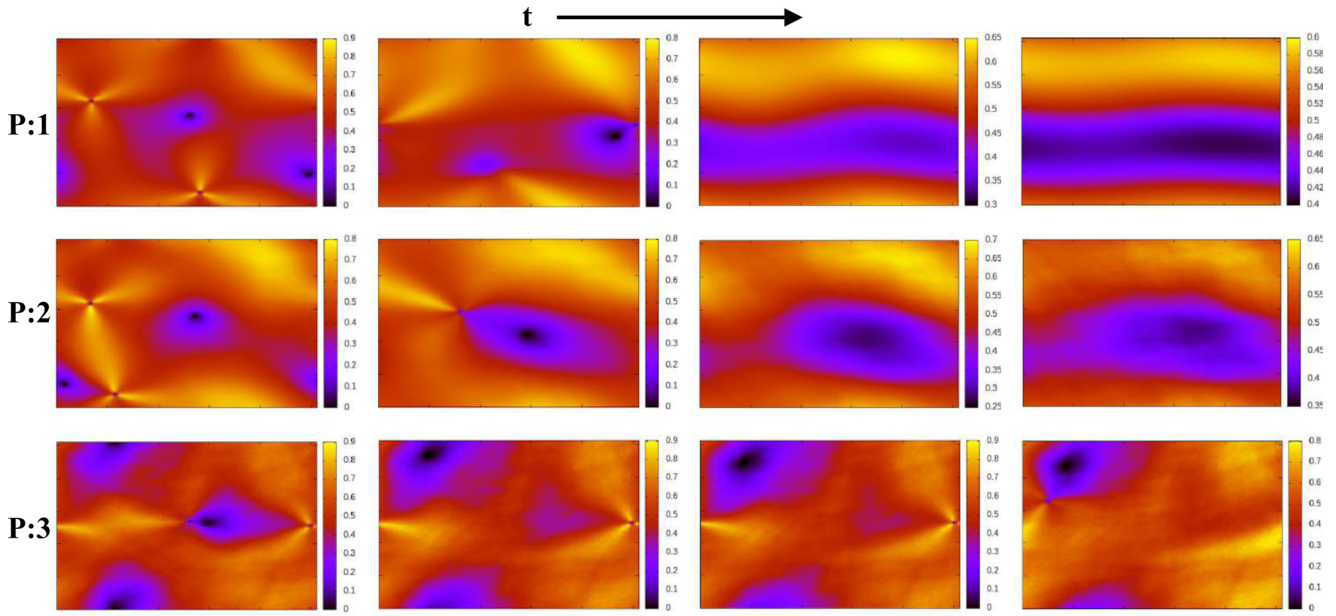

FIG. 8. Snapshots of local NOP, $\mathcal{Q}$ for $a_0 = 0.2$ and for different disorder strength in the system. From top to bottom panel (P:1 to P:3) $h_0 = 0.0$, 0.05, and 0.1, respectively. Snapshots are generated at equal intervals, i.e., $t = 150\,000,\ 300\,000,\ 450\,000,$ and $600\,000$, from left to right, respectively. Notice the numbers on the color bars.

system; distinct domains can be seen as the fluctuation in angular orientation $\Delta\theta$ represented by color bar varies significantly throughout the space whereas, for the clean system, the whole space is identical in terms of $\Delta\theta$. Also, for larger activity $a_0 = 0.3$, the magnitude of $\Delta\theta$ fluctuations decreases, which confirms the stronger intradomain ordering as found in $P(\Delta\theta)$.

2. Fixed a_0 and varying h_0

In Fig. 8, we show the snapshots for local NOP, $\mathcal{Q}$ at different simulation time for $a_0 = 0.2$ and different strengths of disorder in the system. We also included the multimedia files in the SM (see the Supplemental Material [37] for the animations of the nematic order parameter) for the same. We observe that, as we increase the disorder in the system, dynamics of defect slows down. Also, for high disorder, defects

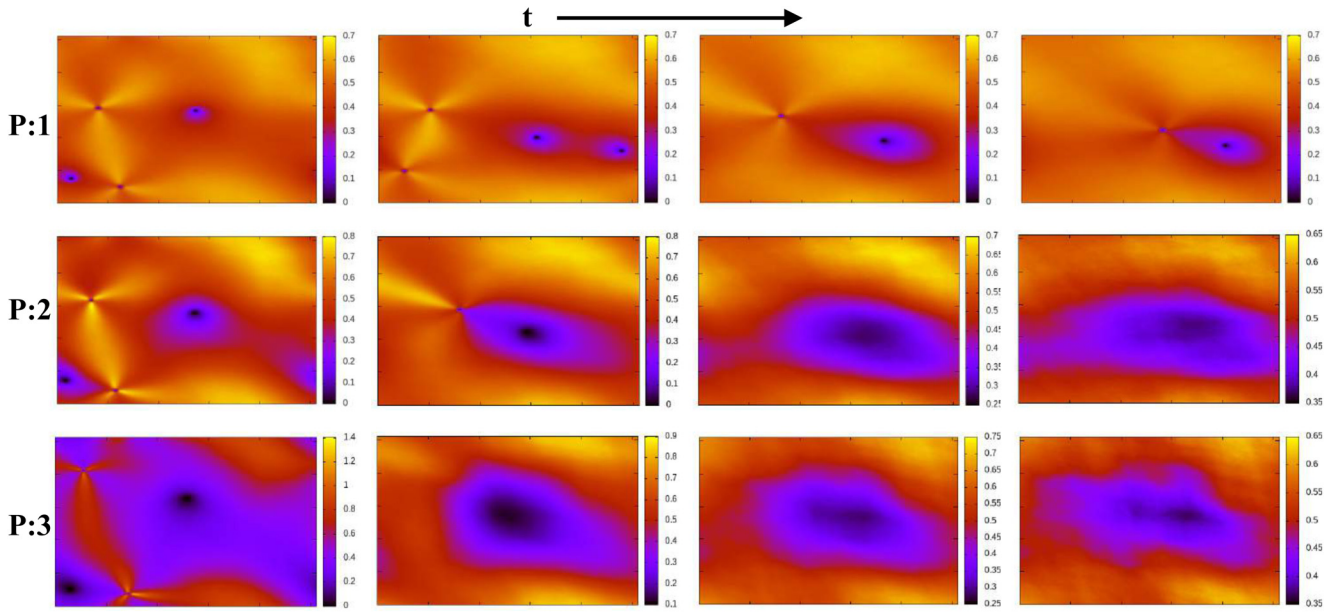

FIG. 9. Snapshots of local NOP, $\mathcal{Q}$ for $h_0 = 0.05$ and for different activity in the system. From top to bottom panel (P:1 to P:3) $a_0 = 0.1$, 0.2, and 0.3, respectively. Snapshots are generated at equal intervals, i.e., $t = 150\,000,\ 300\,000,\ 450\,000,$ and $600\,000$, from left to right, respectively. Notice the numbers on the color bars.

are pinned, which is responsible for the formation of multiple smaller domains as shown in Figs. 1(c) and 7(i)–7(iii).

3. Fixed disorder h_0 and varying activity a_0

Further, we change activity a_0 in Eq. (1) (main text) and plot the snapshots of local NOP, $\mathcal{Q}$ for fixed $h_0 = 0.05$ in Fig. 9 (see the Supplemental Material [37] for animations of the nematic order parameter). We find that, for a fixed h_0 (=0.05 in this case), as we increase a_0, annihilation of defects happens faster than that for the smaller a_0. We also plot the relative separation $\Delta r(t)$ between $+1/2$ and $-1/2$ defects vs t in Fig. 10(a) for three different $a_0 = 0.1$, 0.2, and 0.3. Also the relative speed, which is defined as $u = |\frac{d}{dt}\Delta r(t)| \times 10^{-3}$, is plotted in Fig. 10(b).

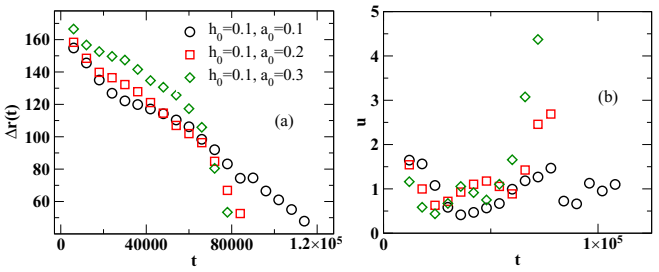

FIG. 10. (a) Relative separation $\Delta(r)$ between $+1/2$ and $-1/2$ defects pair vs time plot and (b) relative speed, $u = |\frac{d}{dt}\Delta r(t)| \times 10^{-3}$, of $\pm 1/2$ defects, for different values of a_0 and fixed $h_0 = 0.1$. t is the simulation time.

[1] C. J. O. Reichhardt and C. Reichhardt, Nat. Phys. **13**, 10 (2017).
[2] A. Morin, N. Desreumaux, J. B. Caussin, and D. Bartolo, Nat. Phys. **13**, 63 (2017).
[3] R. Das, M. Kumar, and S. Mishra, Phys. Rev. E **98**, 060602(R) (2018).
[4] J. Toner, N. Guttenberg, and Y. Tu, Phys. Rev. Lett. **121**, 248002 (2018).
[5] J. Toner, N. Guttenberg, and Y. Tu, Phys. Rev. E **98**, 062604 (2018).
[6] O. Chepizhko, E. G. Altmann, and F. Peruani, Phys. Rev. Lett. **110**, 238101 (2013).
[7] A. Maitra, Phys. Rev. E **101**, 012605 (2020).
[8] C. Dombrowski, L. Cisneros, S. Chatkaew, R. E. Goldstein, and J. O. Kessler, Phys. Rev. Lett. **93**, 098103 (2004).
[9] T. Sanchez, D. T. Chen, S. J. Decamp, M. Heymann, and Z. Dogic, Nature (London) **491**, 431 (2012).
[10] Y. Sumino, K. H. Nagai, Y. Shitaka, D. Tanaka, K. Yoshikawa, H. Chaté, and K. Oiwa, Nature (London) **483**, 448 (2012).
[11] Y. Imry and S. K. Ma, Phys. Rev. Lett. **35**, 1399 (1975).
[12] M. Rotunno, M. Buscaglia, C. Chiccoli, F. Mantegazza, P. Pasini, T. Bellini, and C. Zannoni, Phys. Rev. Lett. **94**, 097802 (2005).
[13] D. L. Blair, T. Neicu, and A. Kudrolli, Phys. Rev. E **67**, 031303 (2003).
[14] A. Sokolov, I. S. Aranson, J. O. Kessler, and R. E. Goldstein, Phys. Rev. Lett. **98**, 158102 (2007).
[15] R. Komkemer, D. Kling, D. Kaufmann, and H. Gruler, Eur. Phys. J. E **1**, 215 (2000).
[16] L. H. Cisneros, J. O. Kessler, S. Ganguly, and R. E. Goldstein, Phys. Rev. E **83**, 061907 (2011).
[17] G. Duclos, C. Erlenkämper, J. F. Joanny, and P. Silberzan, Nat. Phys. **13**, 58 (2017).
[18] K. Kawaguchi, R. Kageyama, and M. Sano, Nature (London) **545**, 327 (2017).
[19] T. B. Saw, A. Doostmohammadi, V. Nier, L. Kocgozlu, S. Thampi, Y. Toyama, P. Marcq, C. T. Lim, J. M. Yeomans, and B. Ladoux, Nature (London) **544**, 212 (2017).
[20] C. Blanch-Mercader, V. Yashunsky, S. Garcia, G. Duclos, L. Giomi, and P. Silberzan, Phys. Rev. Lett. **120**, 208101 (2018).
[21] A. Doostmohammadi, S. P. Thampi, and J. M. Yeomans, Phys. Rev. Lett. **117**, 048102 (2016).
[22] D. Dell'Arciprete, M. L. Blow, A. T. Brown, F. D. Farrell, J. S. Lintuvuori, A. F. McVey, D. Marenduzzo, and W. C. Poon, Nat. Commun. **9**, 1 (2018).
[23] Y. I. Yaman, E. Demir, R. Vetter, and A. Kocabas, Nat. Commun. **10**, 2285 (2019).
[24] H. Li, X. qing Shi, M. Huang, X. Chen, M. Xiao, C. Liu, H. Chaté, and H. P. Zhang, Proc. Natl. Acad. Sci. (USA) **116**, 777 (2019).
[25] E. Bertin, H. Chaté, F. Ginelli, S. Mishra, A. Peshkov, and S. Ramaswamy, New J. Phys. **15**, 085032 (2013).
[26] H. Chaté, F. Ginelli, and R. Montagne, Phys. Rev. Lett. **96**, 180602 (2006).
[27] S. Ramaswamy, R. A. Simha, and J. Toner, Europhys. Lett. **62**, 196 (2003).
[28] A. Doostmohammadi, J. Ignés-Mullol, J. M. Yeomans, and F. Sagués, Nat. Commun. **9**, 3246 (2018).
[29] S. Mishra and S. Ramaswamy, Phys. Rev. Lett. **97**, 090602 (2006).
[30] A. J. Bray, Adv. Phys. **43**, 357 (1994).
[31] P. de Gennes and J. Prost, *The Physics of Liquid Crystals*, International Series of Monographs (Clarendon Press, Oxford, 1993).
[32] L. Giomi, M. J. Bowick, X. Ma, and M. C. Marchetti, Phys. Rev. Lett. **110**, 228101 (2013).
[33] X.-q. Shi and Y.-q. Ma, arXiv:1011.5408.
[34] R. Das, M. Kumar, and S. Mishra, Sci. Rep. **7**, 1 (2017).
[35] X. Q. Shi and Y. Q. Ma, Nat. Commun. **4**, 3013 (2013).
[36] X. Q. Shi, H. Chaté, and Y. Q. Ma, New J. Phys. **16**, 035003 (2014).
[37] See Supplemental Material at http://link.aps.org/supplemental/10.1103/PhysRevE.102.052609 for animations of the nematic order parameter.
[38] A. J. Vromans and L. Giomi, Soft Matter **12**, 6490 (2016).
[39] V. Narayan, S. Ramaswamy, and N. Menon, Science **317**, 105 (2007).
[40] S. Mishra, S. Puri, and S. Ramaswamy, Philos. Trans. R. Soc. A **372**, 20130364 (2014).
[41] A. N. Pargellis, P. Finn, J. W. Goodby, P. Panizza, B. Yurke, and P. E. Cladis, Phys. Rev. A **46**, 7765 (1992).

[42] B. Yurke, A. N. Pargellis, T. Kovacs, and D. A. Huse, Phys. Rev. E **47**, 1525 (1993).
[43] D. Das and M. Barma, Phys. Rev. Lett. **85**, 1602 (2000).
[44] P. M. Chaikin and T. C. Lubensky, *Principles of Condensed Matter Physics* (Cambridge University Press, Cambridge, UK, 1995).
[45] P. G. de Gennes and J. Prost, *The Physics of Liquid Crystals* (Clarendon Press, Oxford, 1993).
[46] G. B. Arfken and H. J. Weber, *Mathematical Methods for Physics* (Elsevier Academic Press, Amsterdam, 2012), pp. 675–739.
[47] L. Giomi, L. Mahadevan, B. Chakraborty, and M. F. Hagan, Phys. Rev. Lett. **106**, 218101 (2011).
[48] L. Giomi, L. Mahadevan, B. Chakraborty, and M. F. Hagan, Nonlinearity **25**, 2245 (2012).